Journal of Non-Crystalline Solids 378 (2013) 135–138

Contents lists available at ScienceDirect

Journal of Non-Crystalline Solids

journal homepage: www.elsevier.com/ locate/ jnoncrysol

Crystallization kinetics of $Al_{86}Ni_8Gd_6$ amorphous alloy

T.V. Kulikova [a], V.A. Bykov [a], A.A. Belozerova [a], A.M. Murzakaev [b,c], R.E. Ryltsev [a,*]

[a] Institute of Metallurgy, Ural Division of Russian Academy of Sciences, Amudsena str. 101, 620016 Ekaterinburg, Russia
[b] Institute of Electrophysics, Ural Division of Russian Academy of Sciences, Amudsena str. 106, 620016 Ekaterinburg, Russia
[c] Ural Federal University named after First President of Russia B.N. Yeltsin, Mira str. 19, 620002 Ekaterinburg, Russia

ARTICLE INFO

Article history:
Received 4 May 2013
Received in revised form 30 May 2013
Available online 20 July 2013

Keywords:
Amorphous alloy;
Cluster structure;
Crystallization kinetics;
Competing reaction;
Non-linear regression

ABSTRACT

We study structure and crystallization kinetics of melt-spun $Al_{86}Ni_8Gd_6$ amorphous alloy. The X-ray diffraction and transmission electron microscopy detect pronounced nanoscale clusters in the structure of the amorphous state. Differential scanning calorimetry analysis shows complex three-stage crystallization of the amorphous alloy at different heating rates. The high temperature X-ray diffraction analysis reveals crystallization mechanism with competing reactions of intermetallic compounds formation. Summarizing the experimental data, we introduce multiversion non-linear kinetic model that describes the crystallization process completely and allows us to determine kinetic parameters with high accuracy. The activation energies obtained reveal relatively stable amorphous state.

1. Introduction

Since their discovery in the 1980s [1–3], the aluminum-based metallic glasses have demanded increasing attention due to their remarkable physical and chemical properties. The ternary Al–TM–RE (TM = transition metal, RE = rare earth) amorphous alloys are among the most important systems of this type because of their unique mechanical properties and capability of the nanocrystallization during thermal annealing [1–7].

In order to control the properties of nanocrystal composite, it is necessary to understand the mechanisms of crystallization processes taking place during annealing and determine their kinetic parameters. It is well known that crystallization of amorphous Al–TM–RE alloys usually proceeds in several stages [8–10] but their clear interpretation is often complicated. Moreover, the mechanism of nanocrystal phase formation for these alloys is still the matter of debates [11–17].

The $Al_{86}Ni_8Gd_6$ alloy we studied belongs to an important class of aluminum-rich Al–TM–RE alloys demonstrating high glass-forming ability and nanocrystallization [18–20]. This compound has been already studied in [18] but its crystallization kinetics and complete picture of transformations have not been clarified yet.

In order to investigate crystallization of the alloy under consideration, the combination of different methods is performed. First of all, we use X-ray diffraction (XRD) analysis and transmission electron microscopy (TEM) to make sure that our samples are completely amorphous. Then we perform differential scanning calorimetry (DSC) analysis at different heating rates to investigate thermal characteristics of crystallization and use high temperature XRD analysis for interpretation of structural transformations. In order to obtain kinetic coefficients corresponding to different stages of crystallization, we use both Kissenger method and non-linear regression kinetic modeling. It allows us to confirm the picture proposed on the base of DSC and XRD data and obtain the kinetic parameters with high accuracy.

2. Experimental procedure

In order to make amorphous ribbons, the alloy with composition $Al_{86}Ni_8Gd_6$ has been preliminarily prepared by the arc-melting technique in argon atmosphere. The purity of the alloy components was (in % wt.): aluminum — 99.99; gadolinium — 99.9; electrolytic nickel — 99.96. The alloy was re-melted three times to improve its homogeneity. The oxide film was mechanically removed from the surface of the samples. Then the specimen prepared was put into a quartz tube and placed in induction furnace of spinning ribbon equipment. The vacuum chamber was previously evacuated and filled with argon up to the pressure of 10 Pa. The melt was heated to 1580–1600 K and then injected on the water-cooled copper roller rotating at a speed of 32 m/s. The amorphous ribbons obtained were about 5 mm width and 35 μm thick.

Primary analysis of amorphous ribbons was performed on X-ray diffractometer XRD 7000 (Shimadzu, Japan) with Cu-Kα radiation and graphite monochromator. For high temperature XRD investigation we used diffractometer D8 ADVANCE (Cu-Kα radiation, position-sensitive detector VANTEC-1, β filter) equipped by high temperature camera XRK 900 (Anton Paar). To control partial oxygen pressure, we applied ceramic electrochemical cell with automatic control system.

During the high temperature XRD analysis, the amorphous ribbons were heated from 543 K up to 723 K at heating rate of 0.3 K/s

* Corresponding author. Tel.: +7 9086377871.
E-mail address: rrylcev@mail.ru (R.E. Ryltsev).

0022-3093/$ – see front matter © 2013 Elsevier B.V. All rights reserved.
http://dx.doi.org/10.1016/j.jnoncrysol.2013.06.019

with the step of 5 K and isothermal soaking of 20 min. for shooting. The phase analysis and crystallographic parameters determination were performed using DIFFRAC^{plus} package and PDF4+ ICCD database of International Center for Diffraction Data.

For TEM analysis, we used transmission electron microscope JEOL 200 kV (Japan) with point resolution of 0.23 nm.

The thermal characteristics of ribbons crystallization were studied by using Netzsch STA 449C calorimeter. The ribbons were continuously heated up to 1273 K at rates of 5, 10, and 20 K/min. Thermal measurements were performed under argon atmosphere (50 ml/min) and calibrated by the melting points of pure indium, tin, bismuth, aluminum, and gold. The accuracy of determining the temperatures and heats of reactions were ±0.2 K and ±5% respectively.

3. Experimental results

For primary control of the quenched alloy structure, we use XRD analysis. According to XRD, the $Al_{86}Ni_8Gd_6$ ribbons are completely amorphous that is confirmed by the broad symmetric peak on XRD pattern (see Fig. 1). It is interesting that well-defined prepeak, usually related with chemically ordered clusters [21,22], is also detected.

To be sure that the specimens do not contain any crystalline inclusions, we perform TEM analysis that confirms that the ribbons are completely amorphous (Fig. 2). It should be noted that TEM also reveals the presence of disordered nanoscale clusters in amorphous phase. The mean size of these clusters is about 3–5 nm that is in close agreement with the estimation of coherence length $l_{coh} \sim 2\pi/\Delta Q$ (where ΔQ is the half-width of the XRD prepeak) obtained from the diffraction data.

Thus, the XRD and TEM data demonstrate the existence of pronounced cluster structure of $Al_{86}Ni_8Gd_6$ amorphous alloy. This result agrees with the conjecture concerning the electronic structure and chemical short-range order of Al–RE-based alloys which was suggested in [23–25]. The detailed investigation of this issue is the matter of separate work.

In order to study thermal and kinetic characteristics of amorphous alloy crystallization we perform DSC analysis at different heating rates v_h. The rates of 5, 10 and 20 K/min were used. According to the results of DSC, the alloy exhibits a three steps crystallization process at all heating rates (Fig. 3). The same crystallization behavior was discovered in [9,10,18] and so it seems to be universal feature of Al — Ni — Gd alloys.

The crystallization temperatures depend on v_h predictably: the higher heating rate we use the higher transition temperatures take place. The glass transition temperature T_g is not fixed that is consistent with the results of [18].

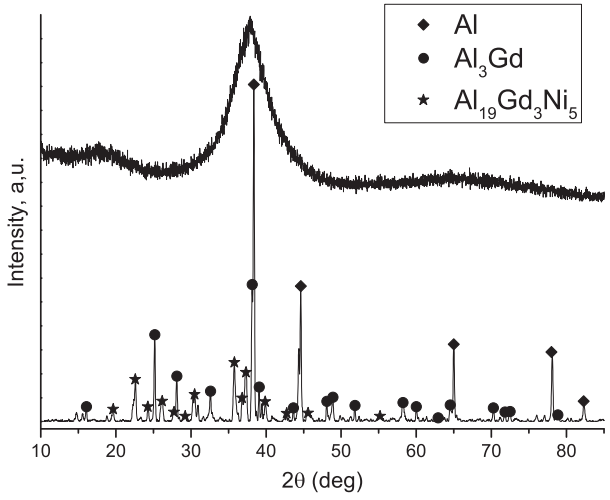

Fig. 1. XRD patterns of amorphous (upper) and final crystal (lower) states of $Al_{86}Ni_8Gd_6$ alloy.

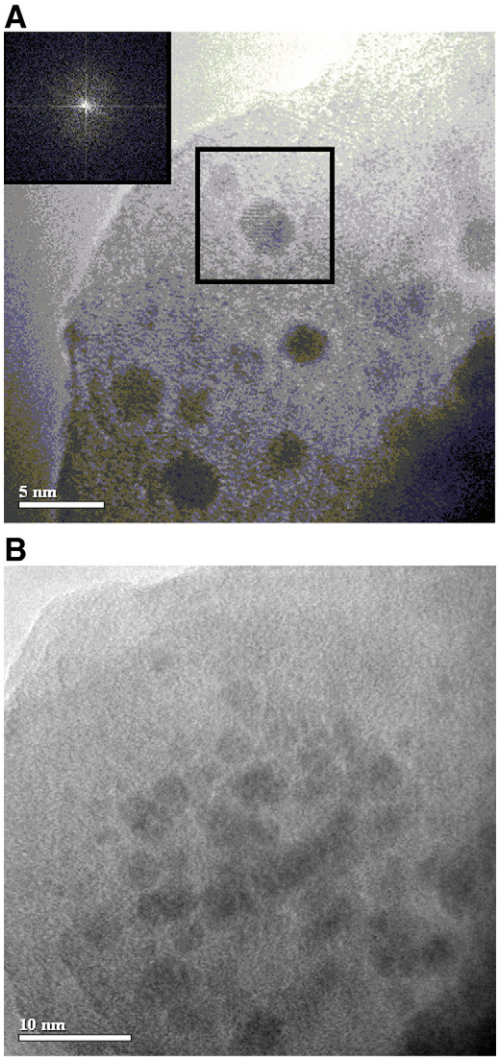

Fig. 2. TEM images of amorphous $Al_{86}Ni_8Gd_6$ alloy with different resolutions. In the insert, the Fourier transform image of the bordered area is shown.

The absence of essential overlapping of DSC peaks corresponding to different crystallization stages allows us to analyze the characteristics of each stage separately. The temperatures of crystallization processes T_{x_i} and corresponding heats ΔH_{x_i} (where $i = (1,2,3)$ is the number of peak) are determined from DSC curves at each heating rate (see Table 1).

In order to understand structural transformations corresponding to each DSC peak, we have performed high temperature XRD analysis. It is found out that the first crystallization stage corresponds to nucleation and growth of aluminum matrix and continues up to 573 K. Then, the complex competing reaction of intermetallic compounds formation takes place (see Fig. 4). The final crystal state of the annealed alloy is composed by aluminum matrix and the most stable compounds $Gd_3Ni_5Al_{19}$ and $GdAl_4$. The intermetallic compounds $Gd_4Ni_6Al_{23}$, $GdAl_4$(O) and $GdAl_4$(T) turned out to be unstable ones and completely disappeared during annealing. So we conclude that second and third crystallization peaks basically correspond to the formation of $Gd_3Ni_5Al_{19}$ and $GdAl_4$ compounds respectively.

4. Kinetic modeling

In most cases, the kinetics of amorphous alloys crystallization is described by using model-free approaches based on isoconversional

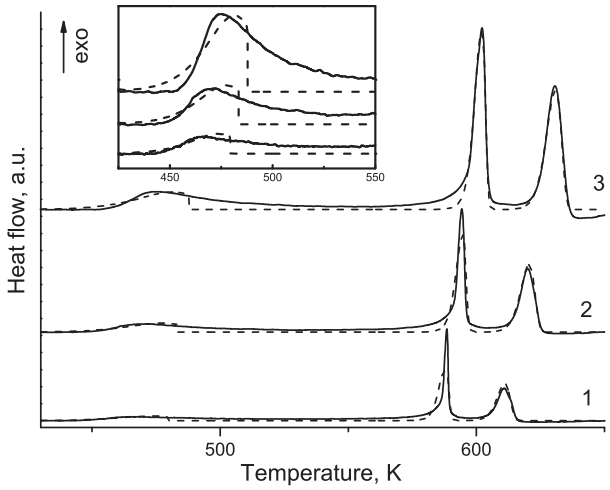

Fig. 3. DSC curves (solid) and their non-linear regression fitting (dash) for amorphous $Al_{86}Ni_8Gd_6$ alloy at different heating rates: (1) — 5, (2) — 10 and (3) — 20 K/min respectively. The insert shows the vicinities of the first peaks.

principle. This principle reads that, at the constant fractional conversion α, the rate of a reaction depends only on the temperature. It allows to obtain kinetic parameters of the reaction by measuring the dependence of one of its characteristics (for example, the temperature corresponding to the maximum of DSC curve) on reaction rate [26–29]. Because of simplicity of model-free methods, they are used in the majority of works devoted to crystallization kinetics of Al–TM–RE amorphous alloys [30,31]. The model-based kinetic description of such alloys is used much more rarely and usually the linear regression approximation is applied [32]. In the frames of both the model-free approaches and the linear regression modeling, a multistage reaction is considered as sequence of independent processes and each of them is analyzed separately. However, in the case of essentially correlated processes (for example, competing reactions in our system) this approach is not valid. In this case, the non-linear regression kinetic modeling considering multistage crystallization as inseparable correlated process is more reasonable approach.

For verification of the results, the combined using of isoconversional and model-fitting approaches is often employed [33]. So we apply two independent methods: model-free analysis based on Kissinger method and non-linear regression kinetic modeling.

4.1. Kissinger method

According to Kissinger method [34], we consider each crystallization stage i as first order chemical reaction and obtain its kinetic parameters (activation energy E_i and pre-exponential factor A_i) from the rate dependence of temperature T_{m_i} corresponding to maximum of i-th DSC peak. The Kissinger equation has the form:

$$\ln\left(v_h/T_m^2\right) = \ln A - E/RT_m, \tag{1}$$

where R is the gas constant. Plotting the dependence of $\ln v_h/T_m^2$ on $1000/T$ for each DSC peak, we get straight lines (Fig. 5) whose

Table 1
Temperatures and heats for each crystallization stage of amorphous $Al_{86}Ni_8Gd_6$ alloy at different heating rates v_h.

v_h (K/min)	T_{x_i} (K)			ΔH_{x_i} (J/g)		
5	449.9	585.6	610.5	9.6	40.2	28.3
10	455.1	589.7	616.2	11.8	42.8	33.8
20	459.4	594.1	627.7	12.86	42.7	35.1

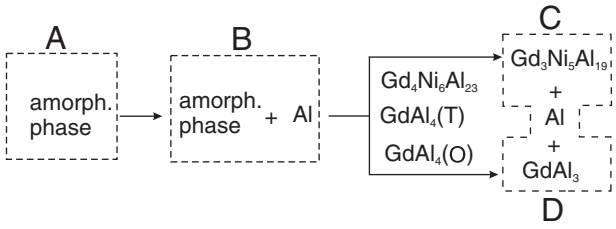

Fig. 4. The sequence of crystallization transformations for amorphous $Al_{86}Ni_8Gd_6$ alloy according to XRD analysis. The intermetallic compounds $Gd_4Ni_6Al_{23}$, $GdAl_4$(O) and $GdAl_4$(T) are unstable and disappear during annealing. The arrows and bordered blocks reflex general scheme for kinetic analysis. The forked arrows indicate competing reaction.

parameters give us activation energies and pre-exponential factors for correspondent crystallization stage (see Table 2).

4.2. Non-linear regression kinetic modeling

With the results of DSC, XRD and TEM, we can build kinetic model describing the crystallization process of amorphous $Al_{86}Ni_8Gd_6$ alloys completely. For that purpose, we use non-linear regression modeling approach realized in Thermokinetics Netzsch-Gerätebau GmbH packet.

As follows from TEM and XRD analysis, the first crystallization stage is primary nucleation and growth of aluminum matrix. So this stage can be described by classical Avrami–Erofeev model [35–37]:

$$\alpha = 1 - \exp\left(-kt^n\right), \tag{2}$$

where α is the fractional conversion; t is time; k is the reaction rate constant; n is the parameter depending on the nucleation geometry and the type of the process [37]. In our case, the growth of aluminum matrix proceeds as three-dimensional process so we put $n = 3$.

The XRD analysis shows that second and first crystallization stages proceed as competing reactions with formation of several intermetallic compounds. The catalysts of these reactions are the regions of aluminum phase. So we describe these stages by Prout–Tompkins equation of heterogeneous autocatalytic reaction [38,39]:

$$\ln\left(\frac{\alpha}{1-\alpha}\right) = k_b t, \tag{3}$$

where k_b is the constant describing reaction branching process.

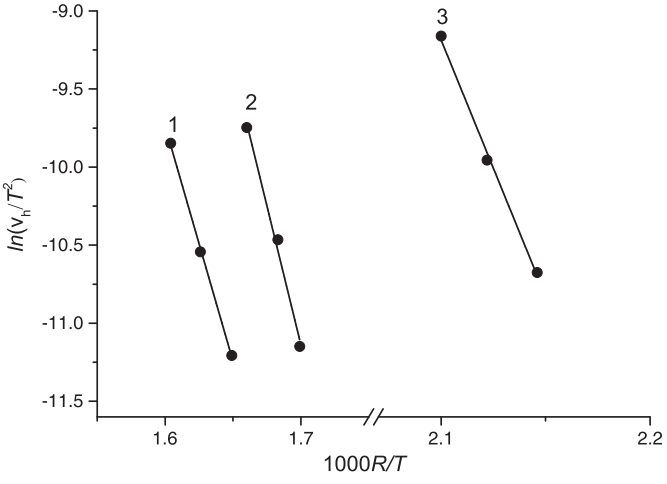

Fig. 5. Kissinger plots of $\ln v_h/T_m^2$ vs. $1000/T$ for each DSC peak of amorphous $Al_{86}Ni_8Gd_6$ alloy. The number of line corresponds to crystallization stage.

Table 2
Kinetic crystallization parameters of amorphous $Al_{86}Ni_8Gd_6$ alloy obtained by Kissinger method and non-linear regression modeling.

	E_i (kJ/mol)			$\ln A_i$ (s^{-1})		
Kissinger method	336	295	218	35.5	24.3	16.3
Non-linear modeling	349	299	218	36.6	25.9	17.7

The temperature dependencies of the rate constants in Eqs. (2) and (3) are assumed to be Arrhenian ones and so the set of kinetic parameters is the same as for Kissinger method.

The general scheme of the kinetic model applied is shown in Fig. 4. In the course of non-linear regression modeling, we determine the kinetic parameters in Eqs. (2), and (3) for each crystallization stage by fitting of whole experimental DSC curve. The proposed model describes the experimental data with high correlation coefficient of 0.9992 and reveals good fitting of experimental DSC curve (Fig. 3). The derived kinetic coefficients are presented in Table 2. The comparison of kinetic coefficients obtained by different methods demonstrates their good correlation that suggests the kinetic model was chosen reasonably. Activation energy E_1 for the first crystallization stage corresponding to primary nucleation and growth of aluminum matrix is the highest one that indicates relatively stable amorphous structure. The same conclusion was made in [30] for Al–Ni–Sm alloy.

5. Conclusions

In summary, we have studied structure and crystallization kinetics of amorphous $Al_{86}Ni_8Gd_6$ alloys by using XRD, TEM, DSC and kinetic modeling methods. The pronounced nanoscale clusters have been detected in the amorphous alloy structure (Fig. 2). We find three-stage crystallization of amorphous alloy: the nucleation and growth of aluminum matrix are followed by the intermetallic compounds formation which is basically contributed by competing reaction between $Gd_3Ni_5Al_{19}$ and $GdAl_4$ (see Fig. 4). The Kissinger method and the non-linear regression kinetic modeling are performed for describing of crystallization kinetics. The results are in close correlation with each other and regression DSC curves fit experimental ones rather well (Fig. 3). The obtained activation energies indicate high stability against nucleation. The discovered peculiarities of structure and crystallization kinetics of amorphous $Al_{86}Ni_8Gd_6$ alloy are consistent with general conception concerning the structural nature of aluminum-based metallic glasses and their thermal stability [40].

Acknowledgments

The work was supported by Russian Foundation for Basic Research (grants 12-03-00757, 11-03-00469 and 12-03-313999). We are grateful to R. Zakharov, S. Petrova, S. Pryanichnikov for XRD analysis and S. Uporov for helpful discussion.

References

[1] Y. He, S.J. Poon, G.J. Shiflet, Science 241 (1988) 1640–1642.
[2] Y. He, S.J. Poon, G.J. Shiflet, Scr. Metall. 22 (1988) 1813–1816.
[3] A. Inoue, K. Ohtera, A.P. Tsai, T. Masumoto, Jpn. J. Appl. Phys. Lett. 27 (1988) L280–L282.
[4] A. Inoue, Prog. Mater. Sci. 43 (1998) 365–520.
[5] G. Hoekstra, S.B. Qadri, R. John, et al., Adv. Eng. Mater. 7 (2005) 805–809.
[6] E. Sansoucy, G.E. Kim, A.L. Moran, B. Jodoin, J. Therm. Spray Technol. 16 (5–6) (2007) 651–660.
[7] M.E. Goldman, N. Unlu, G.J. Shiflet, J.R. Scully, Electrochem. Solid-State Lett. 8 (2) (2005) B1–B2.
[8] V. Ronto, L. Battezzati, A.R. Yavari, M. Tonegaru, N. Lupu, G. Heunen, Scr. Mater. 50 (2004) 839–843.
[9] M.C. Gao, G.J. Shiflet, Scr. Mater. 53 (2005) 1129–1134.
[10] M.C. Gao, G.J. Shiflet, Intermetallics 10 (2002) 1131–1139.
[11] K. Nakazato, Y. Kawamura, A.P. Tsai, A. Inoue, T. Masumoto, Appl. Phys. Lett. 63 (1993) 2644–2646.
[12] A. Inoue, K. Nakazato, Y. Kawamura, A.P. Tsai, T. Masumoto, Mater. Trans. JIM 35 (1994) 95–102.
[13] J.C. Foley, D.R. Allen, J.H. Perepezko, Scr. Mater. 35 (1996) 655–660.
[14] S. Omata, Y. Tanaka, T. Ishida, A. Sato, A. Inoue, Philos. Mag. A 76 (1997) 387–412.
[15] A.P. Tsai, T. Kamiyama, Y. Kawamura, A. Inoue, T. Masumoto, Acta Mater. 45 (1997) 1477–1487.
[16] K.F. Kelton, Acta Mater. 48 (2000) 1967–1980.
[17] K.F. Kelton, Philos. Mag. Lett. 77 (1998) 337–343.
[18] F.Q. Guo, S.J. Poon, G.J. Shiflet, Scr. Mater. 43 (2000) 1089–1095.
[19] M.C. Gao, F. Guo, S.J. Poon, G.J. Shiflet, Mater. Sci. Eng., A 485 (2008) 532–543.
[20] A. Zhu, S.J. Poon, G.J. Shiflet, Scr. Mater. 50 (2004) 1451–1455.
[21] L. Zhang, Y. Wu, X. Bian, H. Li, W. Wang, S. Wu, J. Non-Cryst. Solids 262 (2000) 169–176.
[22] K. Song, X. Bian, X. Lv, J. Guo, G. Li, M. Xie, Mater. Sci. Eng., A 506 (2009) 87–93.
[23] V.E. Sidorov, O.A. Gornov, V.A. Bykov, L.D. Son, V.G. Shevchenko, V.I. Kononenko, K.Yu. Shunyaev, J. Non-Cryst. Solids 353 (32–40) (2007) 3094–3098.
[24] V.E. Sidorov, et al., Mater. Sci. Eng., A 449–451 (2007) 586–589.
[25] R.E. Ryltsev, L.D. Son, Physica B 406 (2011) 3625–3630.
[26] A. Burnham, Thermochim. Acta 355 (2000) 165–170.
[27] B. Roduit, Thermochim. Acta 355 (2000) 171–177.
[28] C. Liu, et al., Polym. Degrad. Stab. 81 (2003) 197–205.
[29] P. Budrugeac, Polym. Degrad. Stab. 93 (2008) 1073–1080.
[30] M. Gogebakan, M. Okumus, Mater. Sci. Pol. 27 (2009) 79–87.
[31] T.P. Ashmi, P. Arun, J. Therm. Anal. Calorim. 105 (2012) 159–165.
[32] A. Revesz, L.K. Varga, S. Surinach, M.D. Baro, J. Mater. Res. 17 (2002) 2140–2146.
[33] I. Dyamant, E. Korin, J. Hormadaly, J. Non-Cryst. Solids 356 (2010) 1784–1790.
[34] H.E. Kissinger, J. Res. Natl. Bur. Stand. 57 (1956) 217–221.
[35] M. Avrami, J. Chem. Phys. 7 (1939) 1103–1112, (8 (1940) 212–224; 9 (1941) 177–184).
[36] B.V. Erofeev, in: J.H. De Boer (Ed.), "Reactivity of Solids", Proc. 4th. Int. Symp. on Reactivity of Solids, Elsevier, Amsterdam, 1960, pp. 273–282.
[37] M.E. Brown, D. Dollimore, A.K. Galway, in: C.H. Bamford, C.F.H. Tipper (Eds.), Comprehensive Chemical Kinetics, vol. 22, Elsevier, Amsterdam, 1980, p. 55.
[38] E.G. Prout, E.C. Tompkins, Trans. Faraday Soc. 40 (1944) 488.
[39] M.E. Brown, Thermochim. Acta 300 (1997) 93–106.
[40] Y. He, S.J. Poon, G.J. Shiflet, Philos. Mag. Lett. 61 (1990) 297–303.